The Plant Cell, Vol. 20: 827–842, April 2008, www.plantcell.org © 2008 American Society of Plant Biologists

RESEARCH ARTICLES

Histone Acetylation and Chromatin Remodeling Are Required for UV-B–Dependent Transcriptional Activation of Regulated Genes in Maize [W]

Paula Casati,[a,1] Mabel Campi,[a] Feixia Chu,[b] Nagi Suzuki,[b] David Maltby,[b] Shenheng Guan,[b] Alma L. Burlingame,[b] and Virginia Walbot[c]

[a] Centro de Estudios Fotosintéticos y Bioquímicos, Facultad de Ciencias Bioquímicas y Farmacéuticas, Universidad Nacional de Rosario, 2000 Rosario, Argentina

[b] Department of Pharmaceutical Chemistry, University of California, San Francisco, California 94143

[c] Department of Biology, Stanford University, Stanford, California 94305

The nuclear proteomes of maize (*Zea mays*) lines that differ in UV-B tolerance were compared by two-dimensional gel electrophoresis after UV light treatment. Differential accumulation of chromatin proteins, particularly histones, constituted the largest class identified by mass spectrometry. UV-B–tolerant landraces and the B73 inbred line show twice as many protein changes as the UV-B–sensitive *b, pl* W23 inbred line and transgenic maize expressing RNA interference constructs directed against chromatin factors. Mass spectrometic analysis of posttranslational modifications on histone proteins demonstrates that UV-B–tolerant lines exhibit greater acetylation on N-terminal tails of histones H3 and H4 after irradiation. These acetylated histones are enriched in the promoter and transcribed regions of the two UV-B–upregulated genes examined; radiation-sensitive lines lack this enrichment. DNase I and micrococcal nuclease hypersensitivity assays indicate that chromatin adopts looser structures around the selected genes in the UV-B–tolerant samples. Chromatin immunoprecipitation experiments identified additional chromatin factor changes associated with the *nfc102* test gene after UV-B treatment in radiation-tolerant lines. Chromatin remodeling is thus shown to be a key process in acclimation to UV-B, and lines deficient in this process are more sensitive to UV-B.

INTRODUCTION

Terrestrial life evolved only after the stratospheric ozone layer formed and could absorb most of the damaging UV-B (280 to 315 nm) in solar radiation (Rozema et al., 2001). Because plants must absorb photons to power photosynthesis, they are inevitably exposed to UV-B (Ballaré et al., 2001; Searles et al., 2001; Paul and Gwynn-Jones, 2003). UV photons cause cellular damage by generating DNA photoproducts and through direct damage to proteins, lipids, and RNA (Britt, 1996; Gerhardt et al., 1999; Casati and Walbot, 2004a). Plant responses to UV-B damage include repair (Waterworth et al., 2002; Bergo et al., 2003) and avoidance (Mazza et al., 2000; Bieza and Lois, 2001). Although much is known about both the perception and the signal transduction pathways modulating responses to visible light, the mechanisms that plants use for sensing and responding to UV-B are largely unknown (Brosche and Strid, 2003; Frohnmeyer and Staiger, 2003; Ulm and Nagy, 2005). Recently, the basic domain/Leu zipper transcription factor long hypocotyl5 (HY5) required for normal growth responses in visible light was identified as an important player in the long-wavelength (300 to 315 nm) UV-B–induced signal transduction cascade in *Arabidopsis thaliana* (Ulm et al., 2004). Upregulation of HY5 is mediated by UVR8, a UV-B–specific factor with sequence similarity to the eukaryotic guanine nucleotide exchange factor RCC1, which is located principally in the nucleus and associates with chromatin via histones (Brown et al., 2005).

Chromatin remodeling is also implicated in the maize (*Zea mays*) response to UV-B, a discovery from transcriptome profiling of lines differing in UV-B sensitivity. Because there is less intervening air mass and greater atmospheric transparency to shorter wavelengths, plants at high altitudes generally experience higher UV-B radiation flux (Madronich et al., 1995). Five maize landraces collected from habitats at altitudes of 2200 to 3600 m have adaptations that increase UV-B tolerance (Casati and Walbot, 2005); they constitutively express higher levels of genes predicted to encode chromatin-remodeling factors than temperate zone maize and also show greater UV-B–mediated upregulation of these genes (Casati et al., 2006). To test the hypothesis that chromatin-remodeling capacity is essential, transgenic plants (in the temperate B73 inbred background) expressing RNA interference (RNAi) to reduce four chromatin factors were found to be acutely sensitive to UV-B at doses that do not cause visible damage to maize lacking flavonoid sunscreens. Symptoms included necrotic sun burning of adult tissue, decreased photosynthetic pigments, altered expression

[1] Address correspondence to casati@cefobi.gov.ar.
The author responsible for distribution of materials integral to the findings presented in this article in accordance with the policy described in the Instructions for Authors (www.plantcell.org) is: Paula Casati (casati@cefobi.gov.ar).

[W] Online version contains Web-only data.

www.plantcell.org/cgi/doi/10.1105/tpc.107.056457

of some UV-B–regulated genes, and seedling lethality (Casati et al., 2006); the RNAi-expressing lines showed no symptoms in visible light. Therefore, chromatin-remodeling capacity is important for effective responses to UV-B and the loss of this capacity is associated with hypersensitivity.

To test whether transcriptome changes are mirrored by protein changes, maize leaf proteins were resolved using two-dimensional (2D) gel electrophoresis (Casati et al., 2005). A total of 163 protein spots altered by UV-B treatment were identified by tandem mass spectrometry (MS/MS); most were related to photosynthesis, stress, or general metabolism. There was an excellent correlation with the predictions based on transcriptome profiling, in which flavonoid-deficient, sensitive lines were shown to express more stress-related transcripts (Casati and Walbot, 2003, 2004b) than standard inbred lines (Blum et al., 2004), as expected if sunscreen pigments attenuate UV-B dosage (Stapleton and Walbot, 1994). Because gel-based proteome approaches detect relatively abundant proteins, few nuclear proteins were identified. To further pursue the connection between UV-B and chromatin-remodeling factors, we report a nuclear- and histone-enriched proteomic analysis to examine the alterations introduced by UV-B radiation in an unbiased, systematic manner. In addition, to link chromatin protein changes with the transcriptome changes observed after UV-B treatments, chromatin immunoprecipitation (ChIP) and nuclease sensitivity assays were used to monitor chromatin status at several UV-B–responsive genes in tolerant and sensitive lines; these assays demonstrate that chromatin-remodeling capacity is fundamental to maize acclimation to UV-B.

RESULTS

Protein Identification and Patterns after UV-B Exposure

Eight maize lines with documented differences in UV-B tolerance were employed. The W23 line is flavonoid sunscreen-deficient, having mutations in the *b* and *pl* genes, which regulate the expression of enzymes in the flavonoid pathway, and it is UV light–sensitive. High-altitude Confite Puneño (origin, Central Andes) and Mishca (origin, Ecuador) lines were selected in their natural environment for UV-B tolerance. Four hypersensitive lines expressing RNAi constructs to reduce the expression of predicted chromatin-remodeling genes were compared with near-isogenic siblings in families segregating 1:1 for control and transgenic plants. The RNAi target genes are as follows: (1) *chc101*, a SWIB domain–containing protein, a potential component of a SWI/SNF complex (Sudarsanam and Winston, 2000); (2) *nfc102*, a putative nucleosome/chromatin assembly factor group C product, highly similar to human retinoblastoma binding protein p48 (also known as Rbap1); (3) *mbd101*, a methyl-CpG binding protein (Grafi et al., 2007); and (4) *sdg102*, a histone methyltransferase with a SET domain.

Greenhouse-grown, 4-week-old plants from each genotype were irradiated for 8 h with UV-B lamps, and adult leaves were harvested for nuclear proteome studies. As controls, plants were exposed under the same lamps covered with a mylar plastic that absorbs UV-B. After all treatments, plants looked healthy. For each treatment, at least three biological replicates of isolated nuclei were evaluated for nuclear enrichment by microscopy and by protein gel blot analysis using antibodies against chloroplastic, mitochondrial, cytosolic, and nucleus-localized proteins (see Supplemental Figure 1 online). Fluorescently labeled proteins (sample 1, Alexa 610; sample 2, Alexa 532) were resolved by isoelectric focusing (IEF) on a 3 to 10 pH gradient and in the second dimension by molecular weight using PAGE. Comparisons are listed in Supplemental Table 1 online. Approximately 500 proteins were resolved on a typical gel; the gels were highly reproducible and had well-resolved spots without streaking. Most spots were present in all genotypes; there were only a few cases in which spots were present in some lines and not in others, and those were analyzed independently. A representative gel in Supplemental Figure 2 online compares control leaf nuclear-enriched proteins (green) with the 8-h UV-B treatment (red) of the Confite landrace. The computer program ImageMaster 2D Platinum (GE Healthcare) was used to detect and quantify protein spots (see Methods). A total of 111 protein spots with differential intensities of at least 1.5-fold after the UV-B treatment from all lines were identified using this software; these are listed in Supplemental Data Set 1 online.

Interpretable MS/MS spectra were obtained for 98 of the 111 differentially accumulated protein spots (see Supplemental Data Set 1 online). Plant processes highlighted by differential protein accumulation are summarized in Figure 1A; identified classes include chaperones, 14-3-3 proteins, stress and signal transduction proteins, and several types of nucleic acid binding proteins. The key finding is that histones constitute the largest functional group modulated by UV-B. Abundance changes of 1.5-fold or greater were found for all histone types: H1-I (2 spots), H2A (2 spots), H2B-1 (2 spots), H2B-2 (10 spots), H2B-3 (2 spots), H3 (5 spots), and H4 (7 spots). Other DNA- and chromatin-associated proteins (see Supplemental Data Set 1 online), such as a histone acetyl-transferase HAC108 and a remorin-type DNA binding protein, were also identified. Several ribosomal proteins were found; this is not surprising, because ribosomes assemble in the nucleus, and we demonstrated previously that UV-B results in cross-linking of RNA to ribosomal proteins, necessitating replacement ribosome synthesis (Casati and Walbot, 2004a). Additionally, some ribosomal proteins have dual roles as transcription factors, such as bacterial protein S4 (Torres et al., 2001) and RPL10, also called QM, a c-Jun–associated factor (Imafuku et al., 1999).

To identify proteins that are regulated or covalently modified by UV-B in a similar way, a hierarchical clustering method was applied. In Figure 1B, the UV-B and no UV-B treatments were compared for all eight maize genotypes. Although many changes are line-specific, reflecting the distinctive germplasm of the two high-altitude lines and of W23, it is clear that UV-B–tolerant lines exhibit more nuclear proteome changes than do sensitive lines: high-altitude Confite (42 protein changes) and Mischa (31) exceed the sensitive W23 line (21 spots). Similarly, the UV-B–tolerant B73 line (40 protein changes) exhibits more changes than the derivative RNAi transgenic lines *nfc102* (20), *sdg102* (20), *chc101* (19), and *mbd101* (15). A few proteins exhibit complex abundance changes that do not correlate with UV-B sensitivity. For example, one form of a remorin protein (Q7XMK5) is increased in W23 after the UV-B treatment, is unchanged in B73, and is decreased in both Confite and Mishca; here,

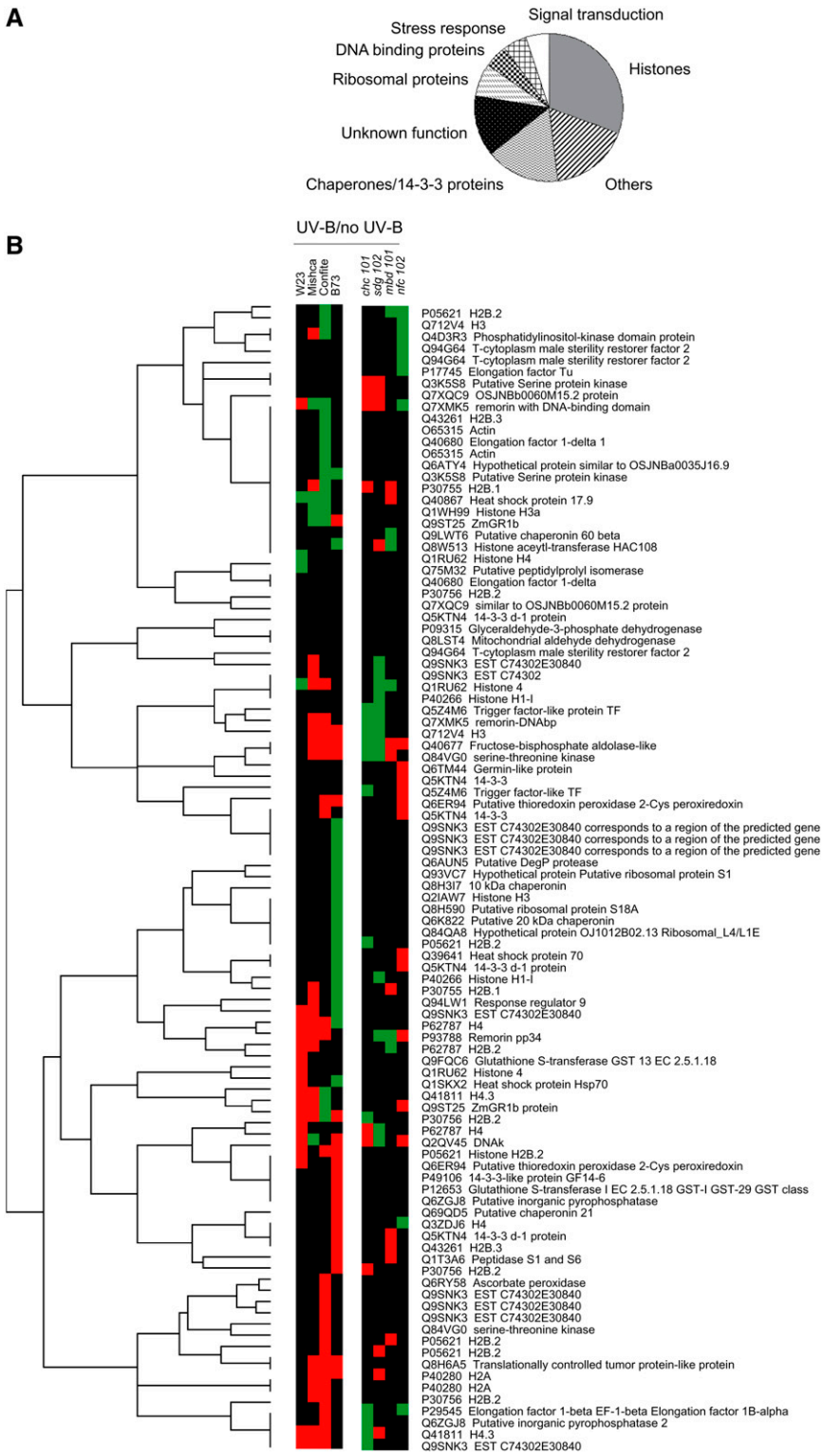

Figure 1. Identification of UV-B–Regulated Putative Nuclear Proteins by 2D Gel Electrophoresis and MS.

(A) Classification of UV-B–regulated nuclear proteins based on putative functions. Proteins with abundances at least 1.5-fold enhanced or decreased after the UV treatment are included.

(B) Hierarchical cluster analysis of leaf nuclear proteins. The proteins included in the analysis were identified in one or more genotypes (W23 *b, pl*, Mishca, Confite Puneño, B73, or RNAi transgenic plants targeted to the *chc101*, *sdg102*, *mbd101*, or *nfc102* gene) after irradiation for 8 h with UV-B supplementation. Proteins from leaves illuminated in the no UV-B treatment were used as references. Clustering was performed according to Eisen et al. (1998). Red indicates higher protein levels than the reference, green indicates lower protein levels than the reference, and black indicates no significant change. The W23 and RNAi transgenic lines are more sensitive to UV-B radiation than B73 and the high-altitude lines Confite and Mishca.

abundance is inversely correlated with UV-B tolerance. However, the same remorin protein form is increased in two of the RNAi knockdown lines (*chc101* and *sdg102*), is decreased in *nfc102*, and is unchanged in *mbd101*, although all four lines are hypersensitive.

Core histones were identified in 30 spots (clustered in Supplemental Figure 3 online). Paralleling the conclusion based on all proteins, more changes are found in the high-altitude lines than in W23 (13 in Confite, 17 in Mishca, and 10 in W23). Similarly, more histone isotypes are differentially accumulated in B73 than in the near-isogenic RNAi transgenic lines (see Supplemental Figure 3 online). For some histones, the same protein was identified in different spots on one gel. For example, Q712V4 histone H3 increased under UV-B in Mishca in one spot but decreased in a second spot (see Supplemental Figure 3 online), and this is true for other histones in additional lines (see Supplemental Figure 3 online). The presence of the same protein type at multiple spots could reflect either differential expression of loci encoding different proteins or posttranslational regulation of the same gene product, a possibility addressed directly by the analysis of histone modification in subsequent experiments. Nonetheless, these initial results suggest that individual lines exhibit different set points with regard to histone expression and/or covalent modification under visible radiation and that they then differentially show discrete patterns of histone types when challenged with UV-B. Importantly, the quantitative difference between tolerant and sensitive lines is clear: during UV-B treatment, tolerant lines exhibit twice as many nuclear protein alterations, including more histone changes, than do sensitive genotypes.

Acetylation at the N-Terminal Tails of Histones H3 and H4 Is Increased in UV-B–Treated Plants

The differential detection of core histone proteins in multiple spots suggests UV-B modulation of histone isoform expression or of posttranslational modifications. Histones are subject to numerous covalent modifications, such as acetylation, methylation, phosphorylation, and ubiquitination, and these modifications control many aspects of chromatin function mediated by histones (Kouzarides, 2007). Dynamic histone modifications are a well-established mechanism to mediate changes in gene expression by altering chromatin structure or by serving as a binding platform to recruit other proteins (Eberharter and Becker, 2002; Jin et al., 2005; Clayton et al., 2006; Li et al., 2007). To analyze histone composition systematically by MS, we acid-extracted histone proteins from UV-B–treated or control B73 leaves and then separated the four core histones by reverse-phase HPLC. A direct comparison of histones H2B, H2A, H4, and H3 at the protein level did not reveal any noticeable difference between the UV-B–treated and control samples. Nevertheless, substantial changes were observed in some low-abundance, acetylated peptides at the N-terminal tails of H4 and H3. The acetylated H4 N-terminal tail (4-GKacGGKacGLGKacGGAKacR-17), for example, gave an *m/z* value at 719.9080 in liquid chromatography–mass spectrometry (LC-MS) (Figure 2A). The sequence of this peptide, as well as the nature and location of the modified residues, were conclusively determined by MS/MS (Figure 2B). Although acetylated and trimethylated Lys residues are isobaric, the mass of this species measured in selected ion monitoring (SIM) mode in Fourier transform-ion cyclotron resonance indicates that all four Lys residues are acetylated (mass accuracy of −3.0 ppm) rather than trimethylated (mass accuracy of 25 ppm for one, 50 ppm for two, 75 ppm for three, and 100 ppm for four trimethylations).

The ion intensity of this acetylated peptide is approximately doubled in UV-B–exposed samples (inset in top panel, Figure 2A) compared with the control (inset in bottom panel), although the discrepancy of total ion intensity in these two samples is ~25% (Figure 2A). This increased abundance of acetylation in the H4 N-terminal tail in UV-B–treated samples is important when comparing with other histone H4 peptides without detected posttranslational modifications (e.g., peptides 68-DAVTYTEHAR-77 and 96-DTLYGFGG-102) or peptides with detected modifications (e.g., unmodified and monomethylated versions of the peptide 24-DNIQGITKPAIR-35) (Figure 2C). Tryptic peptides of histone H3 were analyzed in a similar manner. N-terminal tail acetylated peptide 9-KacSTGGKacAPR-17 was observed to be considerably increased in UV-B–treated samples as well (Figure 2D). In contrast, the level of detected methylations remained essentially unchanged after UV-B treatment (e.g., methylation on Lys-27 detected in peptide 27-KSAPATGGVK-36) (Figure 2D). The error bar on acetylated peptide 9-KacSTGGKacAPR-17 is larger because the peptide had a slightly different retention time in one LC-MS run of the untreated sample, resulting in lower ion intensity for this peptide in one of the replicates. Thus, for both H3 and H4, the differential intensities of various isoforms observed by 2D gel electrophoresis are explained at least in part by posttranslational modification levels that change in response to UV-B treatment, and acetylation in the N-terminal tail of H3 and H4 is the most significantly altered epigenetic mark after UV-B treatment.

Hyperacetylated Histones H3 and H4 Are Present at the Promoter and Transcribed Regions of UV-B–Regulated Genes

To further explore the hypothesis that modified histones contribute to the transcriptional response to UV-B, ChIP analysis was performed using commercially available antibodies specific for acetylated Lys residues in the N-terminal tails of histones H3 and H4 (anti-acetylated H3 and H4 antibodies). Acetylation of H3 and H4 histones is associated with transcriptionally active chromatin (Eberharter and Becker, 2002; Li et al., 2007), and the ChIP assay should thus selectively recover transcribed genes. As a control, antibodies against total H4 histone were used. DNA recovered after immune precipitation was screened via quantitative PCR for the presence of upstream and transcribed regions of *mbd101* and *nfc102* genes (−210 to −441 for *mbd101* and −32 to −277 for *nfc102* upstream regions); both show transcript increases after UV-B treatment (Casati et al., 2006). The coding region of a constitutive thioredoxin-like gene (see Methods) was used as a control, as it is not UV-B–regulated (Casati and Walbot, 2004b). To evaluate nonspecific binding, the quantitative RT-PCR was done with samples incubated in the absence of antibody; all ChIP samples were normalized to total input DNA from sonicated nuclei to evaluate the selective recovery of gene segments.

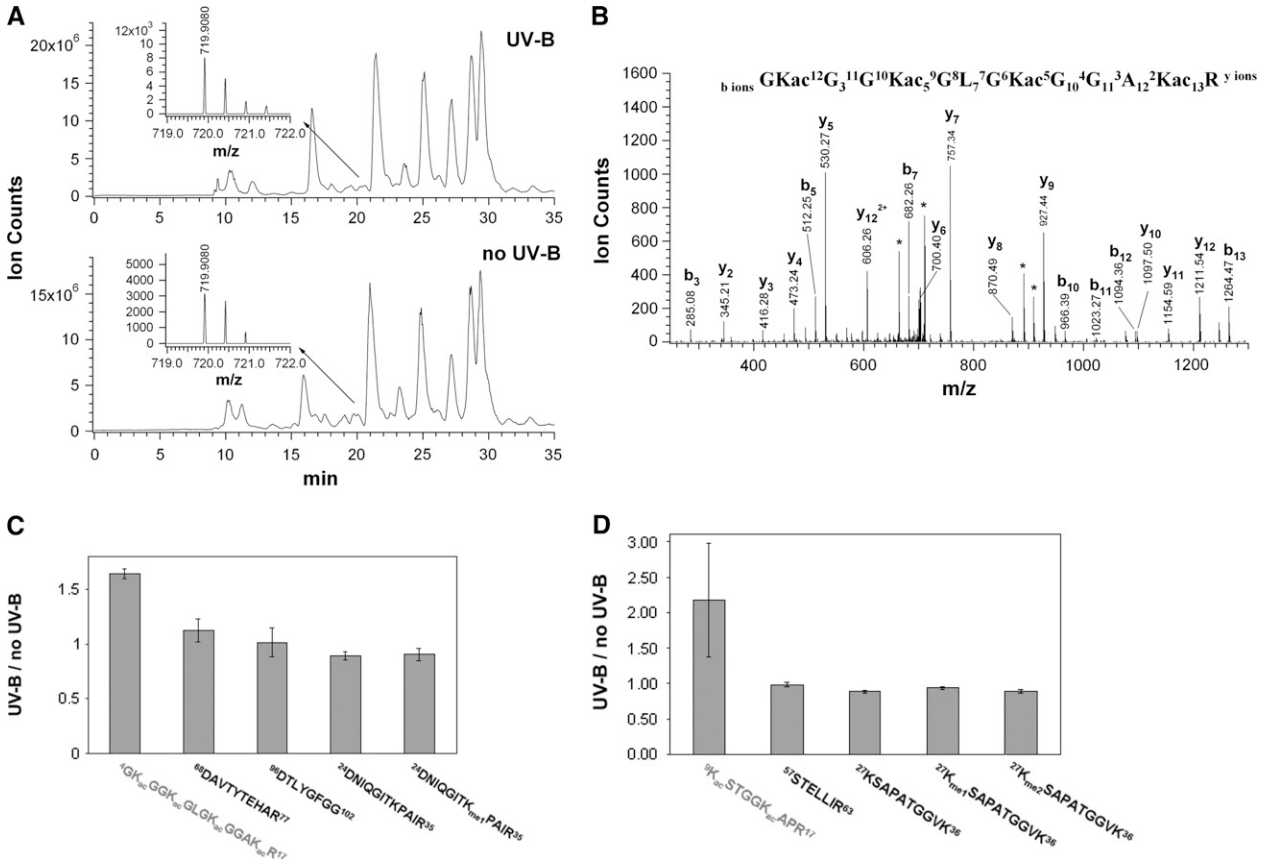

Figure 2. MS Analysis of Purified H3 and H4 Histones.

(A) Total ion chromatograms for the tryptic digestion mixture of histone H4 from UV-B–treated (top panel) or no UV-B (bottom panel) samples. Insets show FT-MS spectra of an acetylated N-terminal tail peptide.

(B) Structure and tandem mass spectrum of the acetylated peptide, 4-GKacGGKacGLGKacGGAKacR-17.

(C) Average ratios of peak areas integrated from LC-MS runs of representative peptides detected from the duplicates of UV-B–treated and no UV-B histone H4. The peptide 4-GKacGGKacGLGKacGGAKacR-17 is more abundant in the UV-B–exposed sample. Values are from two independent experiments, and error bars indicate SE.

(D) Average ratios of peak areas integrated from LC-MS runs of representative peptides detected from the duplicates of UV-B–treated and no UV-B histone H3. The peptide 9-KacSTGGKacAPR-17 is more abundant in the UV-B–exposed sample. Values are from two independent experiments, and error bars indicate SE.

Both upstream and coding regions of *mbd101* and *nfc102* were enriched significantly in the fractions immunoprecipitated with anti-acetylated H3 and H4 antibodies from UV-B–irradiated Confite samples, and similar immunoprecipitated DNA levels were observed for the control thioredoxin-like gene. In contrast, similar levels were measured for most of the upstream and coding sequences of *mbd101* and *nfc102* in W23 samples in the presence or absence of UV-B (Figures 3A and 3B). Some exceptions were also noted, because in the W23 line the UV-B:no UV-B ratio for acetylated H3 and H4 increased significantly in the *mbd101* coding and *mbd101* promoter regions, respectively. No enrichment was detected in the controls (anti-H4 immunoprecipitate or control without antibody [Figure 3C]) for either Confite or W23. Therefore, there is a specific increase in histone acetylation in the promoter and transcribed regions of both Confite genes after UV-B exposure. Figure 3D confirms that *mbd101* and *nfc102* steady state mRNA levels were increased by UV-B in Confite but not in W23. Thus, the increase in acetylation of H3 and H4 by UV-B in this high-altitude line is correlated with an increase in transcript abundance, likely mediated by higher transcription levels.

As a check on this conclusion, the *nfc102* gene was examined in the RNAi *chc101* and *mbd101* transgenic lines, which have decreased transcripts for these target genes (Casati et al., 2006). Figures 4A and 4B show that H3 and H4 acetylation is increased by UV-B in both promoter and transcribed sequences of the *nfc102* gene in B73, but not in the *mbd101* RNAi line or for most of the regions in *chc101* plants, with the exception of a very small increase in H3 acetylation in the promoter of this gene by UV-B. As controls, similar immunoprecipitated DNA levels were detected for the control thioredoxin-like gene and when immunoprecipitation was done using anti-H4 antibodies in all lines and treatments, while there was no enrichment when antibody was omitted during the immunoprecipitation (Figure 4C). Consistent

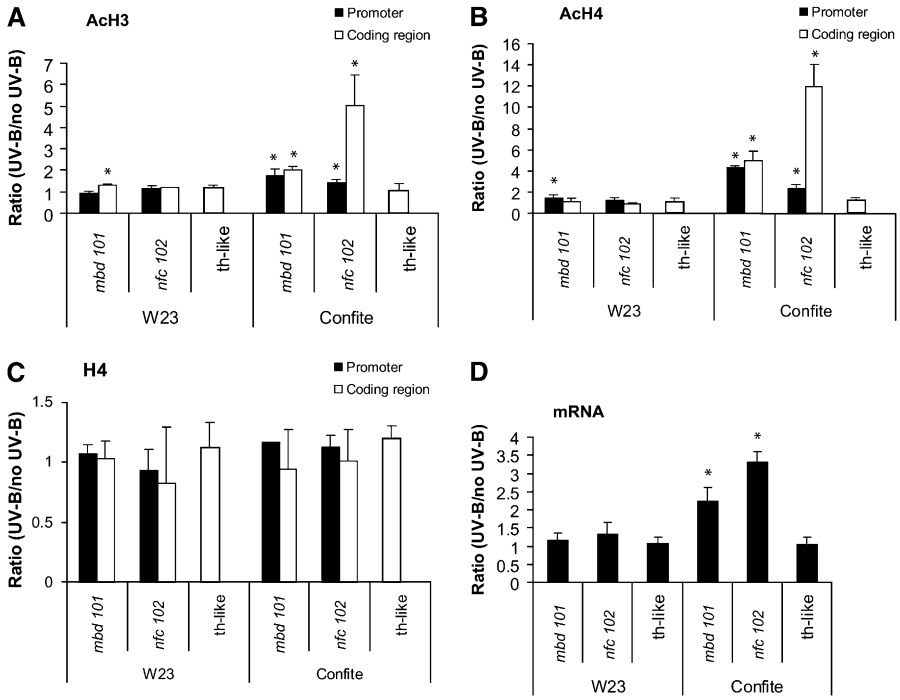

Figure 3. Acetylation State of Histones H3 and H4 Associated with the *mbd101* and *nfc102* Loci.

ChIP assays utilized antibodies specific for N-terminal acetylated histone H3 (**[A]**; AcH3), N-terminal acetylated H4 (**[B]**; AcH4), or total histone H4 (**[C]**; H4) in nuclei prepared from W23 or Confite with UV-B treatment (UV-B) and control conditions (no UV-B). The immunoprecipitates were analyzed for the presence of promoter and transcribed sequences of the target genes *mbd101* and *nfc102* and a transcribed sequence of a control gene that is not UV-B–regulated (th-like) by quantitative PCR. ChIP data were normalized to input DNA before immunoprecipitation. No signal was detected in control reactions (performed for each sample reaction reported above) incubated in the absence of any antibody. Quantitative RT-PCR analysis assessed transcript levels (mRNA) in control and UV-B–treated plants **(D)**. Fifty nanograms of cDNA after reverse transcription of RNA was used. All measurements were done at least in triplicate for each independent preparation. Error bars indicate SE. Statistically significant differences between the UV-B and control treatments (Student's *t* test; $P = 0.05$) are labeled with asterisks.

with the observation in the Confite high-altitude line, increased acetylated histone levels were correlated with increased *nfc102* transcript abundance in B73 (Figure 4D).

ChIP analyses were also conducted for other well-studied UV-B–regulated genes in plants, such as *c2* (a chalcone synthase) and *bz1* (a flavonol 3-*O*-glucosyltransferase). The products of both genes participate in the synthesis of flavonoids and anthocyanins that protect the plants against UV-B (Dooner, 1983). Increased acetylation in H3 and H4 was observed in the promoter regions of both genes in the Confite and B73 lines, which correlated with increased transcription after the UV-B treatment (see Supplemental Figure 4 online). There was no increase in transcript levels in W23, as expected because this line is deficient in the B and Pl transcription factors that regulate the expression of these genes (Dooner, 1983); in addition, no increase in the acetylation of H3 and H4 was measured in this line (see Supplemental Figure 4 online). For the *chc101* plants, no increase in *C2* and *Bz1* transcript levels was detected after the UV-B treatment, nor were there changes in the acetylation state of H3 and H4, as observed previously for the *nfc102* gene (Figure 4; see Supplemental Figure 4 online). Collectively, the ChIP analyses indicate that increased H3 and H4 acetylation occurs in the chromatin region associated with UV-B–regulated maize genes correlated with both increased transcript abundance and UV-B tolerance. The RNAi lines, which have lowered transcript levels of multiple chromatin-remodeling factors, fail to introduce proper posttranslational modifications on histones and do not exhibit differential gene expression of the UV-B–regulated genes examined.

To confirm that chromatin remodeling occurs prior to gene activation, we treated Confite and B73 plants with 100 μM curcumin, an inhibitor of histone acetylation (Balasubramanyam et al., 2004), immediately prior to the UV-B treatment. Then we repeated the ChIP assays using the suite of antibodies. Figure 5 shows that if histone acetylation is impaired, there is no increase in H3 and H4 acetylation in the *nfc102* gene by UV-B; transcript levels of this gene are not significantly increased by UV-B in the lines studied. Thus, blocking a specific aspect of chromatin remodeling, such as histone acetylation prior to the UV-B treatment, dampens the activation of the transcription of *nfc102* by UV-B.

In addition, we analyzed whether other histone covalent modifications correlate with transcript abundance changes in the different maize lines after UV-B treatment. In the MS analysis of acid-extracted histones, we detected that H3 dimethylation in K9 is also increased in UV-B–treated plants. Histone methylation, in particular H3K9me2 and H3K27me2, is a very important

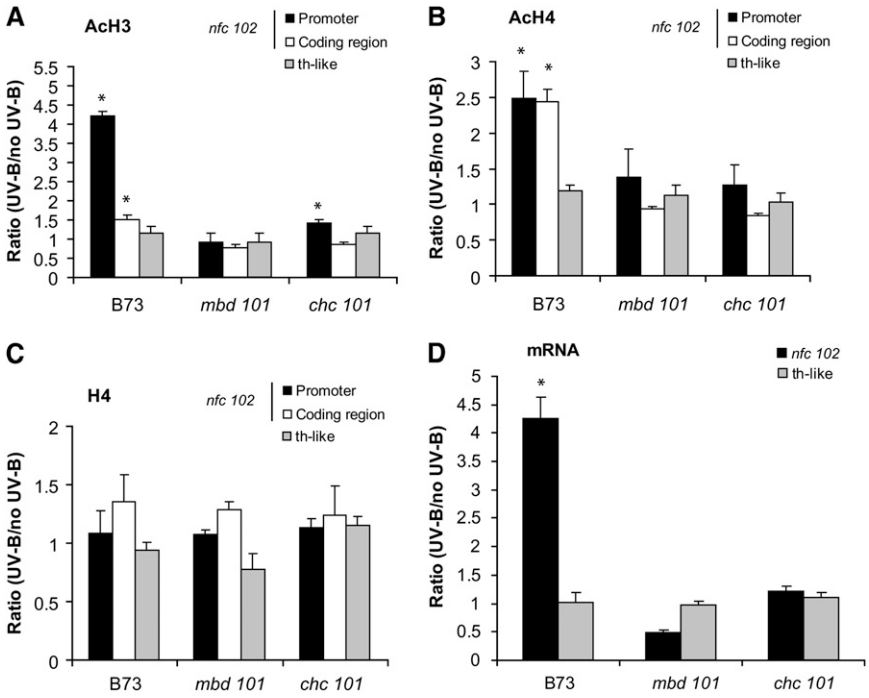

Figure 4. Acetylation State of Histones H3 and H4 Associated with the *nfc102* Gene in Plants Expressing RNAi Knockdown Constructs against *chc101* and *mbd101* Contrasted with Their B73 Nontransgenic Siblings.

Leaf nuclei were prepared from UV-B–treated (UV-B) and control (no UV-B) plants. ChIP assays were done using antibodies specific for acetylated histone H3 (**[A]**; AcH3), acetylated H4 (**[B]**; AcH4), or total histone H4 (**[C]**; H4). The immunoprecipitates were analyzed for the presence of promoter and transcribed sequences of *nfc102* and a transcribed sequence of a control gene that is not UV-B–regulated (th-like) by quantitative PCR. ChIP data were normalized to input DNA before immunoprecipitation. No signal was detected in control reactions (performed for each sample reaction reported above) incubated in the absence of any antibody. Quantitative RT-PCR analysis was also done to study transcript levels (*nfc102* mRNA) in control and UV-B–treated plants **(D)**. Fifty nanograms of cDNA after reverse transcription of RNA was used. All measurements were done at least in triplicate for each of the independent preparations. Error bars indicate SE. Statistically significant differences between the UV-B and control treatments (Student's *t* test; $P = 0.05$) are labeled with asterisks.

epigenetic mark that is usually accompanied by DNA methylation and mediates gene silencing. ChIP analyses were done using antibodies against H3K9me2 and H3K27me2 probing control and UV-B–treated W23, Confite, B73, and *mbd101* plants. Enrichment was analyzed by quantitative PCR with primers for the *nfc102* promoter and coding regions using a thioredoxin-like gene as a control that is not modulated by UV-B (see Supplemental Figure 5 online). Although amplification was very low, there was no significant change in the enriched fractions for either the promoter or the coding region of *nfc102* or for the control gene (see Supplemental Figure 5 online). These results suggest that changes in the methylation of H3 in K9 and K27 do not participate in the regulation of *nfc102* transcription by UV-B; these histone modifications may be involved in other aspects of UV-B responses that are not addressed in our study, such as DNA repair mechanisms.

Nuclease Accessibility of *nfc102* after UV-B Irradiation

The open, or looser, chromatin conformation is observed in many highly transcribed genes, and this property also correlates with chromatin regions with highly acetylated histones (Chua et al., 2001; Li et al., 2007). Therefore, the changes in histone acetylation status and transcript abundance in UV-B–responsive genes observed in maize predict chromatin loosening in UV-B–upregulated genes. To assess chromatin structure directly, we examined the nuclease accessibility of the *nfc102* promoter region. The rates of *nfc102* promoter region degradation by DNase I and micrococcal nuclease were monitored in W23, Confite, B73, and the RNAi *chc101* and *mbd101* transgenic lines in nuclei purified from both control and UV-B–treated leaves. After digestions of 2, 4, 6, 10, or 15 min, DNA was isolated; recovery of the *nfc102* promoter region was determined by quantitative PCR and normalized to the amount of DNA at time 0. A control without nuclease assessed the presence of endogenous nucleases in maize nuclear samples.

For DNase I, which cleaves DNA that is wrapped around the nucleosome at positions where the minor grove faces away from the nucleosome, the rates of degradation in UV-B–treated Confite samples was twice that of the no UV-B treatment samples, showing a 50% decrease after only 2 min of incubation (Figures 6A and 6C). A similar result was observed when B73 samples were used, although the degradation rate was slower (Figures 6A and 6C). By contrast, with or without UV-B treatment,

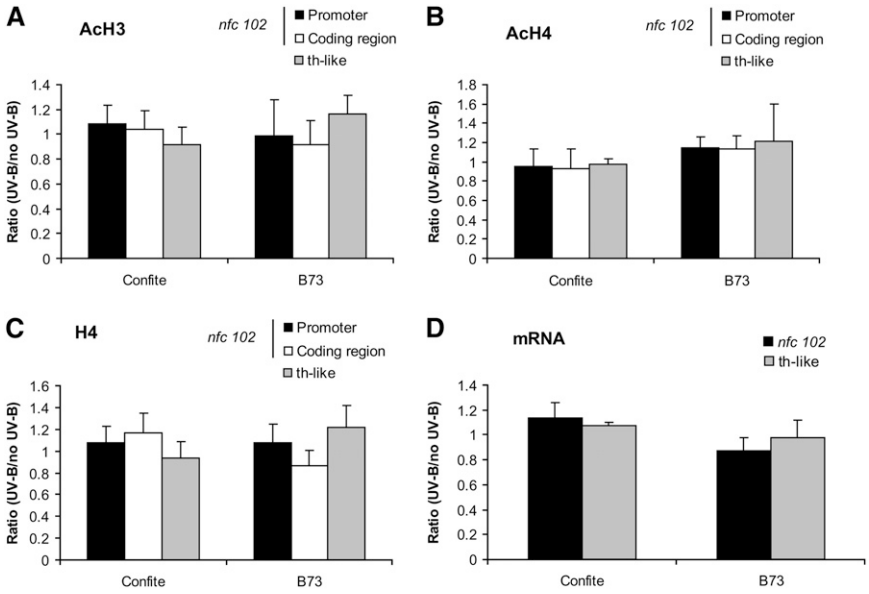

Figure 5. Effects of Curcumin Pretreatment on the Acetylation State of H3 and H4 Histones Associated with the *nfc102* Gene and Its Transcription in Confite and B73 Plants.

Leaf nuclei were prepared from UV-B–exposed (UV-B) and control (no UV-B) plants that were previously treated with curcumin as described in Methods. ChIP assays were done using antibodies specific for acetylated histone H3 (**[A]**; AcH3), acetylated H4 (**[B]**; AcH4), or total histone H4 (**[C]**; H4). The immunoprecipitates were analyzed for the presence of promoter and transcribed sequences of *nfc102* and a transcribed sequence of a control gene that is not UV-B–regulated (th-like) by quantitative PCR. ChIP data were normalized to input DNA before immunoprecipitation. No signal was detected in control reactions (performed for each sample reaction reported above) incubated in the absence of any antibody. Quantitative RT-PCR analysis was also done to study transcript levels (*nfc102* mRNA) in control and UV-B–treated plants **(D)**. Fifty nanograms of cDNA after reverse transcription of RNA was used. All measurements were done at least in triplicate for each of the independent preparations. Error bars indicate SE. None of the comparisons between the UV-B and control treatments showed statistically significant differences (Student's *t* test; $P = 0.05$).

the degradation rates in the flavonoidless W23 and the RNAi *chc101* and *mbd101* DNA samples were similar (Figures 6A and 6C). Therefore, the *nfc102* promoter adopts a more open conformation after UV-B irradiation in Confite, while it is relatively more closed in the three more radiation-sensitive lines. The control thioredoxin-like gene, which is not UV-B–regulated in maize, showed similar degradation rates in assays of samples from both normal illumination– and UV-B–treated W23 and Confite plants (Figures 6B and 6D). The open, or looser, conformation is observed in many highly transcribed genes, and this property also correlates with chromatin regions with highly acetylated histones (Chua et al., 2001; Li et al., 2007). Micrococcal nuclease, which preferentially attacks internucleosomal linker regions (Simpson, 1998), confirmed that the *nfc102* promoter region is selectively more accessible in Confite and B73 samples isolated after UV-B treatment (see Supplemental Figure 6 online): digestion is approximately threefold greater than in the no UV-B control in Confite and twice that in B73 after 2 min. Collectively, these results demonstrate that the UV-B–activated increase in transcripts from the *nfc102* gene is accompanied by increased accessibility to both DNase I and micrococcal nuclease digestion. Combined with the data on differential histone H3 and H4 acetylation, chromatin remodeling to facilitate UV-B–induced transcription is likely a key component of acclimation to this radiation.

The *nfc102* Promoter Associates with Different Chromatin-Remodeling Proteins after UV-B Irradiation

Three commercial antibodies against chromatin-remodeling proteins were found with well-defined specificities for which the antigenic determinant is conserved in maize. To further understand the components of the altered chromatin domain in UV-B–regulated maize genes, we carried out ChIP experiments to monitor CBP acetyltransferase, which can acetylate histones; SWI2/SNF2, a chromatin-remodeling factor that facilitates the binding of gene-specific transcription factors to their DNA targets; and ASH1, the histone methyltransferase specific for H3 Lys-4, which is important in the transcriptional activation of target genes. DNA isolated from immunocomplexes obtained from control and UV-B–treated nuclei from W23, Confite, B73, and the RNAi *chc101* and *mbd101* transgenic plants was used for quantitative PCR using primers specific for the promoter and transcribed regions of the *nfc102* gene and a control thioredoxin-like gene that is not UV-B–regulated.

In ChIP experiments using anti-CBP acetyltransferase antibodies, the promoter region of *nfc102* was enriched in the UV-B–tolerant Confite and B73 samples after irradiation, while no differences were observed between control and treated samples in the UV-B–sensitive genotypes studied (Figure 7A). These results are in accord with the increased histone acetylation within promoter sequences in Confite and B73 reported in Figures 3

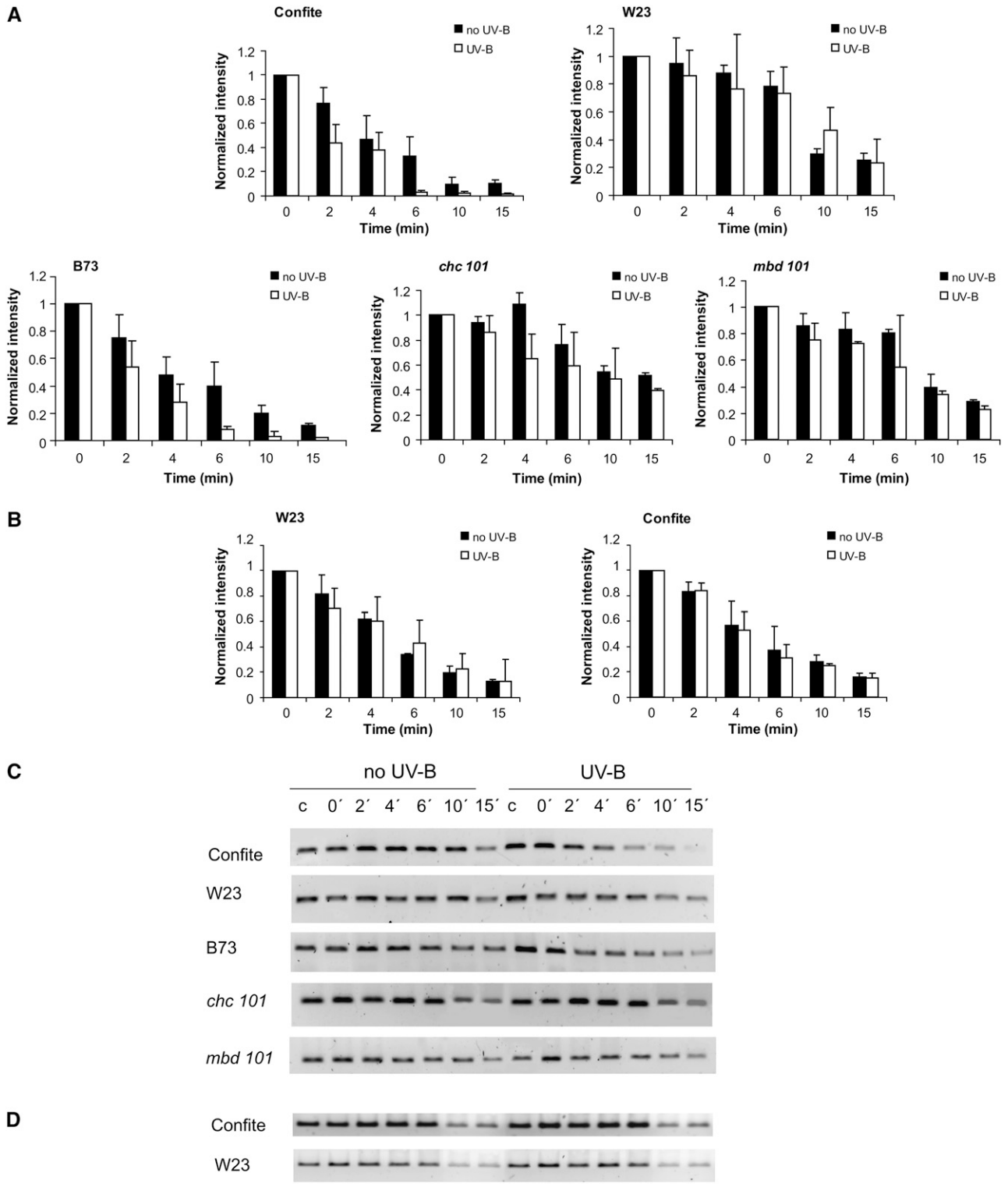

Figure 6. Accessibility of the Promoter Region of the *nfc102* Gene to DNase I.

Nuclei from UV-B–treated (UV-B) and control (no UV-B) plants of the Confite, W23, and B73 lines plus the *chc101* and *mbd101* RNAi transgenic plants were incubated with DNase I for 2, 4, 6, 10, or 15 min. The amount of DNA sequence remaining at each time was determined by quantitative (**[A]** and **[B]**) and standard (**[C]** and **[D]**) PCR using primers for the *nfc102* promoter (**[A]** and **[C]**) and the thioredoxin-like coding region (**[B]** and **[D]**). In **(A)** and **(B)**, the amount of amplicon was normalized to that present at time 0 and plotted against time to evaluate degradation rates in the samples indicated. In **(C)** and **(D)**, PCR products were separated on 2% agarose gels. Control (c) represents a reaction without added nuclease. All measurements were done using three independent preparations, and three PCR experiments were done using each of these samples.

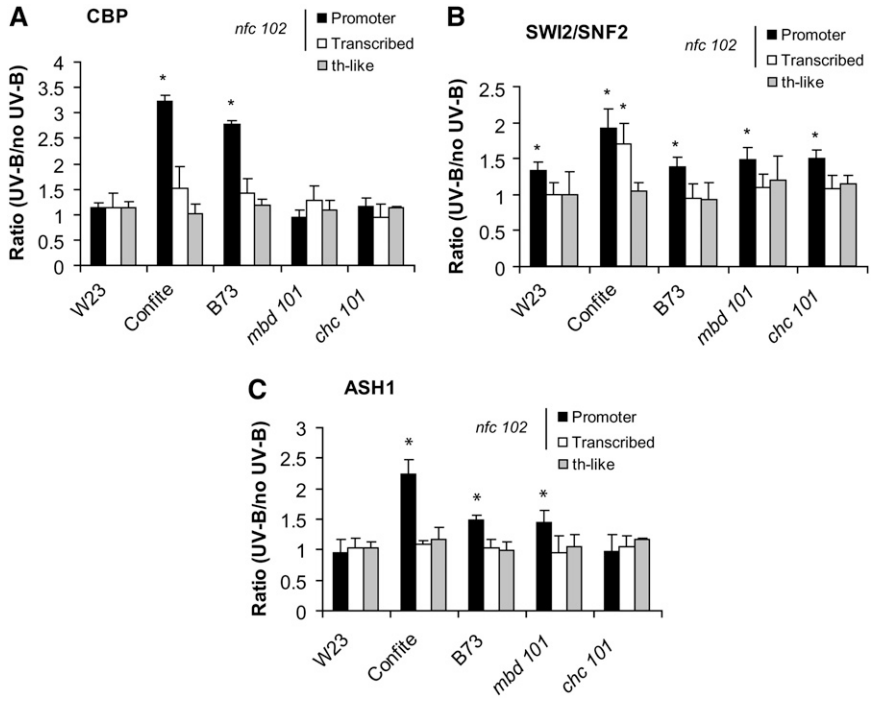

Figure 7. Chromatin-Remodeling Proteins Associated with the *nfc102* Gene.

Nuclei were prepared from W23 and Confite, plus the *chc101* and *mbd101* RNAi transgenic plants and their B73 nontransgenic siblings from both UV-B–treated (UV-B) and control (no UV-B) conditions. ChIP assays employed antibodies specific for a CBP acetyltransferase (**[A]**; CBP), a chromatin-remodeling factor (**[B]**; SWI2/SNF2), and a SET domain protein (**[C]**; ASH1). The immunoprecipitates were analyzed for the presence of promoter and transcribed sequences of *nfc102* and a transcribed sequence of a control gene that is not UV-B–regulated (th-like) by quantitative PCR. ChIP data were normalized to input DNA before immunoprecipitation. No signal was detected in control reactions (performed for each sample reaction reported above) incubated in the absence of any antibody. All measurements were done at least in triplicate using each of three independent preparations. Error bars indicate SE. Statistically significant differences between the UV-B and control treatments (Student's *t* test; $P = 0.05$) are labeled with asterisks.

and 4 and suggest a direct role for a CBP-type acetyltransferase in the modification of maize histones at UV-B–regulated promoters. It is particularly striking that the two maize inbred lines from temperate regions show such distinct responses in this assay: CBP binding in the flavonoid-deficient W23 line is unresponsive to UV-B, while the more UV-B–tolerant B73 line shows an almost threefold increase in promoter association. There is no differential enrichment in the anti-CBP fractions assayed in transcribed regions, suggesting that changes in histone acetylation in these regions (as documented in Figures 3 and 4) may be mediated by other acetyltransferases. Anti-SWI2/SNF2 antibodies detected increased enrichment of DNA promoter sequences after ChIP in all UV-B–treated plants; however, only Confite had a significant change in transcribed regions (Figure 7B). This result suggests an involvement of SWI/SNF in UV-B responses. Using anti-ASH1 antibodies, there is a greater than twofold enrichment of the *nfc102* promoter region in Confite, with less dramatic increases in B73 and *mbd101* (Figure 7C). These additional ChIP assays directed against chromatin-remodeling factors confirm that after UV-B irradiation, the *nfc102* promoter in the UV-B highly tolerant Confite line is associated with higher levels of three types of chromatin-remodeling factors than are the more sensitive lines; to a lesser extent, the B73 promoter is also bound by a different stoichiometry of these factors.

In conclusion, histone posttranslational modifications and chromatin remodeling appear to be intertwining key steps leading to the increased expression of UV-B–activated genes in maize. UV-B–sensitive lines incompetent in these processes show more limited transcript and protein responses to radiation challenge. Considering that UV-B also induces cyclobutane pyrimidine dimers and 6,4 photoadducts in DNA (Britt, 1996) and that chromatin relaxation is required for rapid DNA repair (Thoma, 1999), chromatin remodeling that occurs at UV-B–activated genes may also facilitate the selective repair of genes involved in acclimation responses.

DISCUSSION

Plants use both avoidance and repair to cope with UV-B damage. When acclimation is compromised by mutations in DNA repair (Britt, 1996), downregulation of chromatin-remodeling capacity (Casati et al., 2006), or the absence of sunscreen pigments (Casati and Walbot, 2003), plants are more sensitive to UV-B. Early work on UV-B responses and transcriptome profiling implicated many stress pathways and hormones without defining how UV-B is perceived or how subsequent responses are coordinated. Definition of one pathway linking radiation to acclimation starts with the discovery that UVR8 regulates the

expression of some UV-B–induced genes, including the transcription factor HY5, which controls growth responses in visible light as well as UV-B in *Arabidopsis* (Brown et al., 2005). Maize is intrinsically more resistant to UV-B because it has undergone selection to grow in full sunlight. Nonetheless, plants with decreased expression of four maize chromatin-remodeling components are hypersensitive to UV-B, resulting in seedling lethality, whereas naturally UV-B–resistant high-altitude landraces express higher constitutive and UV-B–inducible levels of transcripts encoding chromatin-associated proteins (Casati et al., 2006). In this report, the linkage between chromatin-remodeling capacity, as reflected in the expression of chromatin-associated proteins, posttranslational modification of histones, and chromatin remodeling at UV-B–upregulated genes, was interrogated by the analysis of adapted high-altitude lines, two temperate inbred lines differing in sensitivity, and four mutants deficient in remodeling factors. Based on the available evidence, modulation of both transcription factors and remodeling of their chromatin templates are required for acclimation to UV-B in flowering plants.

Nuclear protein changes associated with UV-B responses were found by comparing eight maize lines; 111 differentially abundant (1.5-fold or greater difference) proteins were resolved, and 98 of these were identified by MS/MS. Many identified proteins are DNA binding or chromatin factors, including core histones; the total protein and histone isoform changes are a unique signature in each line. Although the two landraces were collected at high altitudes, they are lines of distinct geographic origins and phenotypes, and W23 and B73 are inbred lines derived from different germplasm. Despite the diversity of lines, the quantitative differences are striking between UV-B–tolerant and –sensitive lines. UV-B–tolerant lines exhibit about twice as many nuclear proteome changes as the more sensitive lines. Therefore, the extent or rapidity of altering chromatin at UV-B–regulated genes confers an advantage to thriving in elevated UV-B environments, even if the specific adaptations are unique to each line. In previous studies, the most UV-B–sensitive lines tested showed significant stress responses: the flavonoidless W23 inbred line shows upregulation of many stress-related transcripts, and the RNAi knockdown lines exhibit physiological symptoms, even death, after radiation treatments. Paradoxically, these lines show fewer alterations in the nuclear proteome, in the promoter structure of upregulated genes, and in posttranslational histone modifications than do the UV-B–resistant B73 inbred line and the high-altitude lines. Therefore, successful acclimation to UV-B radiation is distinct from the stress responses to this environmental variable.

Core histones were identified in 30 protein spots in the nuclear proteome analysis (see Supplemental Figure 3 online). The high-altitude lines show more changed histone protein spots than the more UV-B–sensitive line W23, in agreement with previous microarray data (Casati et al., 2006); similarly, B73 exhibits twice as many changes as transgenic siblings expressing RNAi knockdown constructs to one of four predicted chromatin-remodeling genes (Figure 1). A more detailed mass spectrometric analysis of histone proteins revealed that acetylation of histone H3 and H4 N-terminal tails is increased in UV-B–treated B73 plants. Histone acetylation has long been associated with the regulation of gene expression (Eberharter and Becker, 2002; Jin et al., 2005; Clayton et al., 2006); a complex code of histone modifications is proposed to specify alternative chromatin states (Strahl and Allis, 2000; Kouzarides, 2007), with a concomitant profound impact on chromatin-templated processes, including transcription, replication, DNA repair, etc.

To understand more fully the linkage between chromatin changes, in particular histone modifications, the association of proteins with specific genes must be examined. We conducted ChIP experiments using antibodies against N-terminal acetylated H3 and H4 histones. The promoter and transcribed regions of two chromatin-remodeling genes and two flavonoid biosynthetic enzymes that are upregulated by UV-B in tolerant high-altitude Confite and B73 showed increased acetylation states in both H3 and H4 after UV-B treatment. In contrast, the UV-B–sensitive W23 line and transgenic plants expressing RNAi against *chc101* and *mbd101* lack differential H3 and H4 acetylation in most of the upstream and coding sequences of the genes studied after UV-B treatment. These results support the hypothesis that the increased transcript abundances at the four tested loci (and, by extrapolation, other UV-B–activated transcript types) are mediated by the increased transcription rate after the recruitment of transcription activators that recognize acetylated histone tails (Strahl and Allis, 2000). However, it is important to note that in some cases we measured increases in histone acetylation in sensitive lines that are not correlated with changes in transcription (e.g., there is an increase in H4 acetylation in the *mbd101* promoter by UV-B in the W23 line [Figure 3B]); this implies that the increase in histone acetylation does not always correlate with an increase of gene transcription. Thus, the concomitant increases in H3 and H4 acetylation in both promoter and coding regions are probably accompanied by additional types of histone modifications and/or particular histone modification profiles, chromatin-remodeling activities, or additional regulatory factors, which may be required to link the hyperacetylation of histones in UV-B–induced genes in the Confite line to changes in the chromatin accessibility and transcription of these genes. The RNAi knockdown lines are hypersensitive to UV-B; we propose that downregulation of the RNAi targets provokes a modification of the chromatin structure, which thus dampens transcriptional activation by UV-B in these compromised lines. We also demonstrated that nuclease accessibility is highly correlated with H3 and H4 acetylation and with transcript abundance. On the other hand, H3K9me2 and H3K27me2 in the promoter and coding regions of *nfc102* were not changed by UV-B in any of the lines under study; thus, methylation of H3 in K9 and K27 does not participate in the regulation of *nfc102* transcription by UV-B. These histone modifications may be involved in other aspects of UV-B responses that are not addressed in our study, such as DNA repair mechanisms.

In addition to changes in histone acetylation and other covalent modifications, transcriptional activity is ultimately determined by a large suite of chromatin-remodeling and transcription factors. As a first step in defining additional components of the UV-B–mediated responses at specific target genes, ChIP assays were performed using antibodies against a CBP acetyltransferase, SWI2/SNF2, and the SET domain protein ASH1. The largest selective increase

was for precipitation with CBP acetyltransferase antibodies in the UV-B–resistant Confite and B73 samples, which is in accordance with the increase in histone acetylation in the promoter sequences. Interestingly, the enrichment in transcribed regions is not significant with this antibody, suggesting that changes in histone acetylation in transcribed regions may be mediated by a different acetylase(s). In contrast, when antibodies against SWI2/SNF2 were used for ChIP, enrichment of DNA promoter sequences was measured in all UV-B–treated genotypes; this suggests an involvement of SWI/SNF in UV-B responses that could be unrelated to transcriptional activity, such as chromatin remodeling prerequisite for DNA repair. Finally, ASH1 did not show any clear correlation with *nfc102* transcription or with UV-B response.

Nuclease accessibility assays of the *nfc102* promoter after UV-B irradiation showed that degradation rates were higher in Confite and B73 than in UV-B–sensitive lines. Therefore, the *nfc102* promoter adopts a more open conformation after UV-B irradiation in Confite and B73, while it is relatively more closed in the more radiation-sensitive lines. In addition, our data show that chromatin around the *nfc102* promoter of Confite and B73 is generally more accessible than that of the other lines regardless of UV-B illumination, although UV-B increases accessibility (Figure 6). Our results demonstrate that the UV-B–activated increase in transcripts from the *nfc102* gene is accompanied by increased accessibility to both DNase I and micrococcal nuclease digestion. Together with the data on differential histone H3 and H4 acetylation, we can conclude that chromatin remodeling to facilitate UV-B–induced transcription is likely a key component of acclimation to this radiation.

Constitutive chromatin status and remodeling in response to environmental cues are key factors in determining the suite of expressed genes of individuals, and epigenetic programming of gene expression may be transmitted to the next generation through imprinting or chromatin states. For example, the recent report of Molinier et al. (2006) demonstrated that progeny of Arabidopsis plants irradiated with highly mutagenic shortwave UV-C (radiation absent from sunlight) show a persistent increase in homologous recombination, an acclimation response in the treated individuals. In that report, chromatin remodeling was not assessed; however, the linkage between irradiation and heritable altered chromatin states has been established for maize class II transposons of the *MuDR/Mu* family: highly C-methylated elements lose this epigenetic mark during radiation-induced reactivation, and this epigenetic state persists in subsequent generations as long as the elements remain active (reviewed in Walbot and Rudenko, 2002). In our study, we did not detect changes in H3 methylation in histones associated with the *nfc102* gene, so they are probably not involved in the transcriptional activity of this gene by UV-B. With the increasing cases of epigenetic gene regulation, line-specific chromatin status and remodeling capacity are key phenotypes that determine the ability to express genes and the rapidity with which changes in expression can be accomplished. Because UV-B damages DNA directly and both DNA repair and transcriptional changes are required for acclimation, responses to UV-B are more dependent on chromatin-remodeling capacity than are other challenges.

METHODS

Plant Material

The maize (*Zea mays*) high-altitude lines Confite Puneño and Mishca were obtained from the Germplasm Resources Information Network (http://www.ars-grin.gov/cgi-bin/npgs/html/crop.pl); the W23 *b, pl* inbred line is a Walbot laboratory stock. The four RNAi transgenic lines were from the Maize Genetics Stock Center (http://www.aces.uiuc.edu/maize-coop/). The transgenic lines are in a hybrid, mainly B73 background, and each contains an RNAi construct directed toward a specific target gene (http://www.chromdb.org/). For *chc101* plants, stock 3201-01 T-MCG3348.02 was used; for *nfc102*, 3201-07 T-MCG3480.04 was used; for *mbd101*, 3201-11 T-MCG3818.11 was used; and for *sdg102*, 3201-15 T-MCG4268.12, 3201-16 T-MCG4268.16, and 3201-17 T-MCG4268.2 were used. Families for each transgenic line were planted, and resistance to BASTA herbicide was scored; this trait is encoded on the same plasmid as the RNAi expression cassette and hence is a tightly linked marker. The RNAi lines were propagated by pollinating an RNAi carrier with a nontransgenic sibling, resulting in families segregating 1:1 in the subsequent generation. Transgenic plants were validated with three assays: the BASTA herbicide resistance test, PCR detection of the transgene, and verification of reduced target transcript levels using quantitative RT-PCR. Amalgamations of transgenic or nontransgenic siblings from related families segregating for the same RNAi construct were used in some analyses.

Radiation Treatments and Measurements

Plants were grown in a greenhouse with supplemental visible lighting to 1000 $\mu E \cdot m^{-2} \cdot s^{-1}$ with ~15 h of light and 9 h of dark without UV-B for 28 d. UV-B was provided once for 8 h, starting at 3 h after the beginning of the light period, using fixtures mounted 30 cm above the plants (F40UVB 40 W and TL 20 W/12; Phillips) at a UV-B intensity of 2 W/m^{-2} and a UV-A intensity of 0.65 W/m^{-2}. The bulbs were covered by cellulose acetate to exclude wavelengths of <280 nm. As a control, plants were exposed for 8 h under the same lamps covered with polyester film (no UV-B treatment; UV-B, 0.04 W/m^{-2}, UV-A, 0.4 W/m^{-2}). Lamp output was recorded using a UV-B/UV-A radiometer (UV203 A+B radiometer; Macam Photometrics) to ensure that both the bulbs and filters provided the designated UV light dosage in all treatments. Adult leaf samples were collected immediately after irradiation.

For the curcumin experiments, leaves from the different plants were sprayed with a solution of 100 μM curcumin in 100% (v/v) ethanol immediately prior to the UV-B or control treatment.

Nuclear Isolation, Protein Extraction, and Labeling with Alexa 610 and Alexa 532 Dyes

The nuclei enrichment procedure was done as described by Gendrel et al. (2005). Nuclei were further purified on a Percoll gradient according to Slatter et al. (1991). Nuclei were pelleted by centrifugation at 3000*g* for 10 min at 4°C and then resuspended in a buffer containing 30 mM Tris-HCl, pH 8.5, 7 M urea, 2 M thiourea, and 4% CHAPS. After pelleting the debris with a brief low-speed spin, proteins were labeled with succinimidyl ester derivatives of Alexa 610 or Alexa 532 after adjusting the pH to 8.5 (Invitrogen). Proteins were labeled at the ratio 75 μg of protein:60 nmol of Alexa labeling dye in DMSO. After vortexing, samples were incubated for at least 2 h on ice. The reaction was quenched by 1 μL of 1 mM Lys and 20 mM DTT, then 4% (v/v) ampholyte buffers 3 to 10 were added (GE Healthcare).

2D Gel Electrophoresis

Seventy-five micrograms of an Alexa 610–labeled sample was mixed with 75 μg of Alexa 532–labeled protein. A Protean IEF Cell apparatus

(Bio-Rad) was used for IEF with precast immobilized pH gradient strips (pH 3 to 10; linear gradient, 17 cm [Bio-Rad]). Samples (300 μL) containing 75 μg of protein from each sample were loaded by in-gel rehydration. The strips were subjected to IEF for 60,000 V/h. Focused gel strips were equilibrated in SDS equilibration buffer (50 mM Tris-Cl, pH 8.8, 30% glycerol, 2% SDS, and 6 M urea), first with buffer containing 1% (w/v) DTT for 15 min and afterward with buffer containing 4% iodoacetamide for 15 min. The strips were washed briefly with running buffer, loaded on top of a prepared SDS-PAGE Laemmli gel cast with 12.5% acrylamide, and covered with 0.5% agarose. Proteins were separated at 1 W per gel for 12 to 15 h, and the fluorescent images corresponding to Alexa 610 (excitation, 612 nm; emission peak, 628 nm) and to Alexa 532 (excitation, 532 nm; emission peak, 554 mn) were acquired using an EpiChemi3 fluorescent scanner (UVP BioImaging Systems). Data were saved in TIF format. Triplicate gels of biological replicates were run; the dye label was swapped for one gel. To excise samples for MS, a preparative gel loaded with 0.5 mg of total protein was run.

Gel Image Analysis

Images were analyzed using ImageMaster 2D Platinum (GE Healthcare) using the following protocol. Spot detection and background subtraction were performed for each gel image; artifacts (such as dust particles or streaks detected as protein spots) were removed by manual editing. When appropriate, spot chains were manually split into separate entities. A master gel for each treatment was based on the gel containing the most spots to serve as an effective spot index for the analysis of multiple gels. Gels for each replicate were grouped and matched to the master gel. The master gels for each treatment were then rematched. Background detection and normalization were performed again to account for any changes in overall volume caused by manual editing. After all editing and rematching were completed, the images were analyzed for protein spot differences, comparing the relative fluorescence of the two dyes. To compare protein profiles between two samples that had been run on the same gel or between samples run on different gels, a normalization procedure was employed to allow for variation in total protein loading. Total spot volume was calculated, and each spot was assigned a normalized spot volume as a proportion of this total value. Normalized spot volumes were compared between Alexa 610– and Alexa 532–labeled samples on each gel. Excluding spots that were unmatched to the reference gel did not affect the relative quantification of matched spots to a significant extent. Difference thresholds were then applied to identify the protein spots with a statistically significant 1.5-fold difference in normalized spot volume ($P < 0.05$). Results were analyzed using Cluster and Treeview (Eisen et al., 1998; http://genome-www4.stanford.edu/MicroArray/SMD/restech.html). A hierarchical clustergram using the default option with the uncentered correlation similarity metric grouped genes by both related regulation patterns and expression amplitudes.

In-Gel Digestion, MS, and Database Searching

Before spot picking, the gel was stained using Coomassie Brilliant Blue R 250 (0.1% [w/v], 45% [v/v] methanol, and 10% [v/v] acetic acid). The spots that showed 1.5-fold different expression levels in UV-B–treated samples were manually excised and subjected to in-gel digestion (http://donatello.ucsf.edu/ingel.html) with trypsin (porcine, side chain–protected; Promega) as described by Casati et al. (2005). Digested samples were then separated by a self-packed Ultro 120 (5-μm particle size; Peeke Scientific) 150- × 0.1-mm capillary column and analyzed online with either an Applied Biosystems MDS Sciex QSTAR or a Thermo LTQ-FT mass spectrometer operated in data-dependent mode. The flow rate of HPLC was 300 to 330 nL/min, with a gradient from 5 to 50% B in 30 min (A = 0.1% formic acid in HPLC water; B = 0.1% formic acid in acetonitrile). The numbers of unique peptides and sequences found for each protein are listed in Supplemental Data Set 1 online. For some spots, peptide sequences matched to more than one distinct protein. In these cases, spot identities were assigned based on the fit of the theoretical pI and molecular weight of each protein to that derived experimentally from the 2D gels. If an ambiguity arose, the spots corresponding to the same protein from different gels were reanalyzed by MS/MS for clarification.

For acid-extracted samples, approximately 2 μg of histone proteins purified from UV-B–treated and untreated B73 plants was loaded in each lane and separated on a 4 to 20% SDS-PAGE gel. Bands corresponding to core histone proteins were sliced, digested, and analyzed as described previously (Chu et al., 2006). Comparative analysis of histone samples was carried out in duplicate. Digested samples were analyzed by nanoflow LC-MS and LC-MS/MS using a Thermo LTQ-FT mass spectrometer. Data were acquired in a data-dependent mode, and the instrument was cycled in a seven-scan mode (one full FT-MS scan and three pairs of SIM FT scans followed by MS/MS ion-trap scans). SIM mode has a 10-D window with 50,000 resolution, and the accuracy of mass measurements is typically within 5 ppm under such conditions. For the MS quantification of acetylated histones, the peak areas were integrated from each LC-MS run of peptides from two independent experiments. The integrated peak areas of each identified peptide were normalized by the sum of the peak areas of confidently identified peptides in each LC-MS run.

The collision-induced dissociation spectra were submitted for National Center for Biotechnology Information database searching using MASCOT (http://www.matrixscience.com). Although there is robust EST support for ~40,000 maize genes, the maize genome is not completely sequenced. If no significant sequence similarity was found in maize or within the narrow group of flowering plants, all species across taxonomic boundaries were searched. Variable modifications selected for searching include oxidation of Met, N-terminal acetylation, N-terminal pyroglutamine, and modification of Cys residues by carbamidomethylation or polyacrylamide. For samples containing histone proteins, phosphorylation, Lys monomethylation, dimethylation, and trimethylation, Arg monomethylation and dimethylation, and Lys ubiquitination were also taken into consideration for queries. Label-free quantitative comparison of histone peptides was carried out after database searches of the MS/MS spectra from LC-MS runs. Selected ion chromatograms of peptides identified in both LC-MS runs were extracted and integrated.

Immunoblot Analysis

For immunodetection, total proteins were extracted with a buffer containing 100 mM Tris-HCl, pH 7.3, 1 mM EDTA, 10 mM $MgCl_2$, 50 mM KH_2PO_4, 15 mM 2-mercaptoethanol, 20% (v/v) glycerol, and 1 mM phenylmethylsulfonyl fluoride (PMSF). Ten percent (w/v) SDS-PAGE was performed, and proteins were electroblotted onto a nitrocellulose membrane for immunoblotting according to Burnette (1981). Commercial IgG fractions were used for the detection of histone H4 (Abcam). Antibodies against *Amarantus viridis* phosphoenolpyruvate carboxylase were donated by S. Colombo, antibodies to recombinant maize NADP-malic enzyme were from M. Saigo, and antibodies to *A. viridis* NAD-malic enzyme were from J. Berry. Bound antibody was visualized by linking to alkaline phosphatase–conjugated goat anti-rabbit/anti-mouse IgG according to the manufacturer's instructions (Bio-Rad). The molecular masses of the polypeptides were estimated from a plot of the log of the molecular masses of marker standards (Bio-Rad) versus migration distance.

ChIP and Nuclease Digestion

Two grams of control or UV-B–treated maize leaves was fixed with 1% formaldehyde at 22°C for 15 min immediately after harvest under vacuum. Gly (150 μL of 1 M) was added to stop the cross-linking, and the incubation was allowed to proceed for another 5 min. Tissue was rinsed two times with distilled water and was used for isolation of nuclei as

described by Gendrel et al. (2005). Nuclei were collected by centrifugation, suspended in 500 μL of lysis buffer (1% SDS, 10 mM EDTA, 50 mM Tris-HCl, pH 8.0, and 1 mM PMSF), and sonicated five times for 15 s on ice with a Vibra Cell sonicator (Sonics & Materials). Between sonications, the solution was incubated for 5 min on ice. The sonicated solution was then centrifuged at 12,000*g* for 5 min at 4°C. The supernatant was collected and diluted 10-fold with ChIP dilution buffer (1.1% Triton X-100, 1.2 mM EDTA, 16.7 mM Tris-HCl, pH 8.0, and 167 mM NaCl) to give a chromatin solution at the correct ionic concentration for immunoprecipitation. Ten microliters from each sample was divided into aliquots to serve as the input DNA control. Eight hundred microliters of chromatin solution was combined with the following amounts of rabbit antisera: 4 μL of anti-N-terminal acetylated H4, 4 μL of anti-N-terminal acetylated H3 (catalog numbers 06-598 and 06-599, respectively; Upstate Biotechnology), 4 μL of H4 (ab7311), 4 μL of H3 (dimethylated K9; ab1220), 4 μL of H3 (dimethylated K27; ab6002), 4 μL of anti-SWI2/SNF2 (ab5154), 4 μL of anti-ASH1 (ab4477), and 4 μL of anti-CBP (ab18291; Abcam). The commercial antibodies were selected if the epitope used in antibody generation was identical to the target maize protein or contained few mismatches. The solutions were incubated overnight at 4°C on a rotation wheel. After the addition of 40 μL of protein A–Sepharose beads, the chromatin solutions were incubated for at least 1 h at room temperature on the rotation wheel. The beads were washed twice with 500 μL of low-salt wash buffer (0.1% SDS, 1% Triton X-100, 2 mM EDTA, 20 mM Tris-HCl, pH 8.0, and 150 mM NaCl), twice with 500 μL of high-salt wash buffer (0.1% SDS, 1% Triton X-100, 2 mM EDTA, 20 mM Tris-HCl, pH 8.0, and 500 mM NaCl), twice with LiCl wash buffer (0.25 M LiCl, 1% Nonidet P-40, 1% deoxycholate, 1 mM EDTA, and 10 mM Tris-HCl, pH 8.0), and twice with 500 μL of TE (10 mM Tris-HCl, pH 7.5, and 1 mM EDTA). Each wash was 5 min long. The immunocomplexes were eluted from the beads with 500 μL of 1% SDS and 0.1 M $NaHCO_3$, mixed with 20 μL of 5 M NaCl, and heated at 65°C overnight to reverse the formaldehyde cross-linkages. Two microliters of proteinase K (10 mg/mL), 20 μL of 1 M Tris-HCl, pH 6.5, and 10 μL of 0.5 M EDTA were then added to each sample, followed by incubation for 2 h at 42°C. DNA was extracted with phenol:chloroform (1:1, v/v). After precipitation with ethanol, the purified DNA pellets were suspended in 20 μL of distilled water and analyzed by quantitative PCR. Three replicates of ChIP were performed from each genotype/treatment sample type, and three quantitative PCR experiments were done with each sample.

Endonuclease digestion of DNA from purified nuclei was done as described by Chua et al. (2001). For endonuclease digestion, nuclei were isolated according to Gendrel et al. (2005) and resuspended in 1 mL of NSB buffer (50% glycerol, 50 mM Tris-HCl, pH 8.0, 5 mM $MgCl_2$, 2.5 mM DTT, and 0.5 mM PMSF). Nuclease digestions were performed using 320 μL of nuclei in NSB buffer, 480 mL of 30 mM NaCl and 8 mM $CaCl_2$, 160 mL of 50 mM Tris-HCl, pH 8.0, and 5 mM $MgCl_2$, and the endonuclease (0.5 unit/mL for micrococcal nuclease [Fermentas International] and 0.3 unit/mL for DNase I [Promega]). Two 120-μL aliquots were removed from the mixture before the addition of the nuclease to use as the nonnuclease control and for the zero time point. After addition of the endonuclease, the digestion mixture and the nonnuclease control were incubated at 37°C. At 2, 4, 6, 10, and 15 min, aliquots of 120 μL were taken from the digestion mixture and mixed immediately with an equal volume of phenol:chloroform (1:1). After extraction, the DNA was precipitated with ethanol, dried, suspended in 10 μL of water, and analyzed. Three replicates of each nuclease treatment were performed from each genotype/treatment sample type, and three quantitative PCR and PCR experiments were done with each sample.

RNA Isolation and RT Reaction

RNA samples were isolated using Trizol (Invitrogen) as described by Casati and Walbot (2003). RNA was isolated from a pool of top leaves (which received the greatest UV-B exposure) from six plants; pooling minimizes organismal variation. Five micrograms of total RNA from each genotype/treatment combination was used for cDNA synthesis using SuperScript II reverse transcriptase (Invitrogen).

PCR and Quantitative PCR

Primers for the promoter and transcribed regions of maize *nfc102* and *mbd101*, for the promoter regions of *c2* and *bz1*, and for the transcribed region of a thioredoxin-like gene were designed using Primer3 software (Rozen and Skaletsky, 2000). The primer pairs were as follows: promoter region of *mbd101* (AI737448): L, 5′-TACCCGCTGCACACTCTT-3′, R, 5′-ACGTGATCGGTTCATTGC-3′; transcribed region of *mbd101*: L, 5′-ATGCAGAGCCAAATCAGC-3′, R, 5′-AAGGCAGAGGCACAAAAG-3′; promoter region of *nfc102* (AW155846): L, 5′-CAGAGCAAATCGGAGACG-3′, R, 5′-CCGTTCTTTCCCTCCACT-3′; transcribed region of *nfc102*: L, 5′-CATGAGAAGGTTGGGAAGAA-3′, R, 5′-AATTGTCCAAGGATCTGACG-3′; promoter region of *c2* (AY728810): L, 5′-CCGTCCAACTGACCTAACC-3′, R, 5′-GAGCTAGCGATCGAGCTG-3′; promoter region of *bz1* (X13500): L, 5′-CCGTTGATCCCAACAAAC-3′, R, 5′-ACGTGTCCGCTTTATTCC-3′; and for the thioredoxin-like gene (AW927774): F, 5′-GGACCAGAAGATTGCAGAAG-3′, R, 5′-CAGCATAGACAGGAGCAATG-3′. Quantitative PCR was carried out in a MiniOPTICON2 apparatus (MJ Research, a division of Bio-Rad) as described by Casati and Walbot (2004b). The significance of the results was analyzed using Student's *t* test, with significance at $P < 0.05$. For quantitative PCR, three replicates were performed for each sample plus template-free samples and other negative controls (reaction without reverse transcriptase for RT-PCR experiments). To normalize the data, primers for a thioredoxin-like transcript were used. PCR was carried out in the same equipment under the same conditions of quantitative PCR without SYBR Green I, but 20 cycles were done instead of the 40 used in quantitative PCR (Casati and Walbot, 2004b). To confirm the size of the PCR products, and to check that they corresponded to a unique and expected PCR product, the final PCR products were separated on a 2% agarose gel. Previously, these products were sequenced to verify that the product was the correct amplicon (Casati and Walbot, 2004b).

Accession Numbers

Sequence data from this article can be found in the GenBank/EMBL data libraries under the following accession numbers: *nfc102*, AW155846; *mbd101*, AI737448; *c2*, AY728810; *bz1*, X13500; thioredoxin-like gene, AW927774.

Supplemental Data

The following materials are available in the online version of this article.

Supplemental Figure 1. Immunoblot Analysis of Total Cellular and Nuclear Proteins Resolved by 10% SDS-PAGE.

Supplemental Figure 2. Analytical 2D Gel of Confite Leaf Nuclei from Control Plants (No UV-B) or Plants Supplemented with UV-B for 8 h.

Supplemental Figure 3. Hierarchical Cluster Analysis of Histones after 8 h of UV-B Exposure.

Supplemental Figure 4. Acetylation State of Histones H3 and H4 Associated with the *c2* and *bz1* Loci.

Supplemental Figure 5. Methylation State of Histone H3 Associated with the *nfc102* Loci in K9 and K27 Residues.

Supplemental Figure 6. Accessibility of the Promoter Regions of the *nfc102* Gene to Micrococcal Nuclease.

Supplemental Table 1. Samples Compared Directly in the Proteomic Analysis on the Same or Different Gels.

Supplemental Data Set 1. Proteins Regulated by UV-B in Nuclei of Different Maize Genotypes Identified by MS.

ACKNOWLEDGMENTS

The work of P.C., M.C., and V.W. was supported by the National Institutes of Health (Grant R03 TW-07487) funded by the Fogarty International Center. The University of California, San Francisco MS facility is supported by National Institutes of Health Grants RR-01614, RR-015804, RR-012961, and RR-019934 (to A.L.B.). P.C. is a member of the Research Career of the Consejo Nacional de Investigaciones Científicas y Técnicas of Argentina, and M.C. is a doctoral fellow of this council. F.C. is a Rett Syndrome Research Foundation postdoctoral fellow. We thank Dave Skibbe and Zhiyong Wang for helpful comments.

Received October 22, 2007; revised March 19, 2008; accepted March 25, 2008; published April 8, 2008.

REFERENCES

Balasubramanyam, K., Varier, R.A., Altaf, M., Swaminathan, V., Siddappa, N.B., Ranga, U., and Kundu, T.K. (2004). Curcumin, a novel p300/CREB-binding protein-specific inhibitor of acetyltransferase, represses the acetylation of histone/nonhistone proteins and histone acetyltransferase-dependent chromatin transcription. J. Biol. Chem. **279:** 51163–51171.

Ballaré, C.L., Rousseaux, M.C., Searles, P.S., Zaller, J.G., Giordano, C.V., Robson, T.M., Caldwell, M.M., Sala, O.E., and Scopel, A.L. (2001). Impacts of solar ultraviolet-B radiation on terrestrial ecosystems of Tierra del Fuego (southern Argentina)—An overview of recent progress. J. Photochem. Photobiol. B **62:** 67–77.

Bergo, E., Segalla, A., Giacometti, G.M., Tarantino, D., Soave, C., Andreucci, F., and Barbato, R. (2003). Role of visible light in the recovery of photosystem II structure and function from ultraviolet-B stress in higher plants. J. Exp. Bot. **54:** 1665–1673.

Bieza, K., and Lois, R. (2001). An Arabidopsis mutant tolerant to lethal ultraviolet-B levels shows constitutively elevated accumulation of flavonoids and other phenolics. Plant Physiol. **126:** 1105–1115.

Blum, J.E., Casati, P., Walbot, V., and Stapleton, A.E. (2004). Split-plot microarray design allows sensitive detection of expression differences after ultraviolet radiation in the inbred parental lines of a key maize mapping population. Plant Cell Environ. **27:** 1374–1386.

Britt, A.B. (1996). DNA damage and repair in plants. Annu. Rev. Plant Physiol. Plant Mol. Biol. **4:** 75–100.

Brosche, M., and Strid, A. (2003). Molecular events following perception of ultraviolet-B radiation by plants. Physiol. Plant. **117:** 1–10.

Brown, B.A., Cloix, C., Jiang, G.H., Kaiserli, E., Herzyk, P., Kliebenstein, D.J., and Jenkins, G.I. (2005). A UV-B-specific signaling component orchestrates plant UV protection. Proc. Natl. Acad. Sci. USA **102:** 18225–18230.

Burnette, W.N. (1981). Western blotting: Electrophoretic transfer of proteins from sodium dodecyl sulfate–polyacrylamide gels to unmodified nitrocellulose and radiographic detection with antibody and radioiodinated protein A. Anal. Biochem. **112:** 195–203.

Casati, P., Stapleton, A.E., Blum, J.E., and Walbot, V. (2006). Genome-wide analysis of high altitude maize and gene knockdown stocks implicates chromatin remodeling proteins in responses to UV-B. Plant J. **46:** 613–627.

Casati, P., and Walbot, V. (2003). Gene expression profiling in response to ultraviolet radiation in *Zea mays* genotypes with varying flavonoid content. Plant Physiol. **132:** 1739–1754.

Casati, P., and Walbot, V. (2004a). Crosslinking of ribosomal proteins to RNA in maize ribosomes by UV-B and its effects on translation. Plant Physiol. **136:** 3319–3332.

Casati, P., and Walbot, V. (2004b). Rapid transcriptome responses of maize (*Zea mays*) to UV-B in irradiated and shielded tissues. Genome Biol. **5:** R16.

Casati, P., and Walbot, V. (2005). Differential accumulation of maysin and rhamnosylisorientin in leaves of high altitude landraces of maize after UV-B exposure. Plant Cell Environ. **28:** 788–799.

Casati, P., Zhang, X., Burlingame, A.L., and Walbot, V. (2005). Analysis of leaf proteome after UV-B irradiation in maize lines differing in sensitivity. Mol. Cell. Proteomics **4:** 1673–1685.

Chu, F., Nusinow, D.A., Chalkley, R.J., Plath, K., Panning, B., and Burlingame, A.L. (2006). Mapping post-translational modifications of the histone variant MacroH2A1 using tandem mass spectrometry. Mol. Cell. Proteomics **5:** 194–203.

Chua, Y.L., Brown, A.P.C., and Gray, J.C. (2001). Targeted histone acetylation and altered nuclease accessibility over short regions of the pea plastocyanin gene. Plant Cell **13:** 599–612.

Clayton, A.L., Hazzalin, C.A., and Mahadevan, L.C. (2006). Enhanced histone acetylation and transcription: A dynamic perspective. Mol. Cell **23:** 289–296.

Conconi, A., Smerdon, M.J., Howe, G.A., and Ryan, C.A. (1996). The octadecanoid signalling pathway in plants mediates a response to ultraviolet radiation. Nature **383:** 826–829.

Dooner, H.K. (1983). Coordinate genetic regulation of flavonoid biosynthetic enzymes in maize. Mol. Gen. Genet. **189:** 136–141.

Eberharter, A., and Becker, P.B. (2002). Histone acetylation: A switch between repressive and permissive chromatin. EMBO Rep. **3:** 224–229.

Eisen, M.B., Spellman, P.T., Brown, P.O., and Botstein, D. (1998). Cluster analysis and display of genome-wide expression patterns. Proc. Natl. Acad. Sci. USA **95:** 14863–14868.

Frohnmeyer, H., and Staiger, D. (2003). Ultraviolet-B radiation-mediated responses in plants. Balancing damage and protection. Plant Physiol. **133:** 1420–1428.

Gendrel, A.V., Lippman, Z., Martienssen, R., and Colot, V. (2005). Profiling histone modification patterns in plants using genomic tiling microarrays. Nat. Methods **2:** 213–218.

Gerhardt, K.E., Wilson, M.I., and Greenberg, B.M. (1999). Tryptophan photolysis leads to a UVB-induced 66 kDa photoproduct of ribulose-1,5-bisphosphate carboxylase/oxygenase (Rubisco) in vitro and in vivo. Photochem. Photobiol. **70:** 49–56.

Grafi, G., Zemach, A., and Pitto, L. (2007). Methyl-CpG-binding domain (MBD) proteins in plants. Biochim. Biophys. Acta **1769:** 287–294.

Imafuku, I., Masaki, T., Waragai, M., Takeuchi, S., Kawabata, M., Hirai, S.-i., Ohno, S., Nee, L.E., Lippa, C.F., Kanazawa, I., Imagawa, M., and Okazawa, H. (1999). Presenilin 1 suppresses the function of c-Jun homodimers via interaction with QM/Jif-1. J. Cell Biol. **147:** 121–134.

Jin, J., Cai, Y., Li, B., Conaway, R.C., Workman, J.L., Conaway, J.W., and Kusch, T. (2005). In and out: Histone variant exchange in chromatin. Trends Biochem. Sci. **30:** 680–687.

Kouzarides, T. (2007). Chromatin modifications and their function. Cell **128:** 693–705.

Li, B., Carey, M., and Workman, J.L. (2007). The role of chromatin during transcription. Cell **128:** 707–719.

Madronich, S., Mckenzie, R.L., Caldwell, M. and Bjorn, L.O. (1995). Changes in ultraviolet-radiation reaching the earth's surface. Ambio **24:** 143–152.

Mazza, C.A., Boccalandro, H.E., Giordano, C.V., Battista, D., Scopel, A.L., and Ballaré, C.L. (2000). Functional significance and induction by solar radiation of ultraviolet-absorbing sunscreens in field-grown soybean crops. Plant Physiol. **122:** 117–125.

Molinier, J., Ries, G., Zipfel, C., and Hohn, B. (2006). Transgeneration memory of stress in plants. Nature **442:** 1046–1049.

Paul, N.D., and Gwynn-Jones, D. (2003). Ecological roles of solar UV

radiation: Towards an integrated approach. Trends Ecol. Evol. **18:** 48–55.

Rozema, J., Bjorn, L.O., Bornman, J.F., Gaberscik, A., Hader, D.P., Trost, T., Germ, M., Klisch, M., Groniger, A., Searles, P.S., Flint, S.D., and Caldwell, M.M. (2001). A meta analysis of plant field studies simulating stratospheric ozone depletion. Oecologia **127:** 1–10.

Rozen, S., and Skaletsky, H.J. (2000). Primer3 on the WWW for general users and for biologist programmers. In Bioinformatics Methods and Protocols: Methods in Molecular Biology, S.A. Krawetz and S. Misener, eds (Totowa, NJ: Humana Press), pp. 365-386.

Searles, P.S., Kropp, B.R., Flint, S.D., and Caldwell, M.M. (2001). Influence of solar UV-B radiation on peatland microbial communities of southern Argentina. New Phytol. **152:** 213–221.

Simpson, R.T. (1998). Chromatin structure and analysis of mechanisms of activators and repressors. Methods. **15:** 283–294.

Slatter, R.E., Dupree, P., and Gray, J.C. (1991). A scaffold-associated DNA region is located downstream of the pea plastocyanin gene. Plant Cell **3:** 1239–1250.

Stapleton, A.E., and Walbot, V. (1994). Flavonoids can protect maize DNA from the induction of ultraviolet-radiation damage. Plant Physiol. **105:** 881–889.

Strahl, B.D., and Allis, C.D. (2000). The language of covalent histone modifications. Nature **403:** 41–45.

Sudarsanam, P., and Winston, F. (2000). The Swi/Snf family of nucleosome-remodeling complexes and transcriptional control. Trends Genet. **16:** 345–351.

Thoma, F. (1999). Light and dark in chromatin repair: Repair of UV-induced DNA lesions by photolyase and nucleotide excision repair. EMBO J. **18:** 6585–6598.

Torres, M., Condon, C., Balada, J.-M., Squires, C., and Squires, C.L. (2001). Ribosomal protein S4 is a transcription factor with properties remarkably similar to NusA, a protein involved in both non-ribosomal and ribosomal RNA antitermination. EMBO J. **20:** 3811–3820.

Ulm, R., Baumann, A., Oravecz, A., Mate, Z., Adam, E., Oakeley, E.J., Schafer, E., and Nagy, F. (2004). Genome-wide analysis of gene expression reveals function of the bZIP transcription factor HY5 in the UV-B response of Arabidopsis. Proc. Natl. Acad. Sci. USA **101:** 1397–1402.

Ulm, R., and Nagy, F. (2005). Signalling and gene regulation in response to ultraviolet light. Curr. Opin. Plant Biol. **8:** 477–482.

Walbot, V., and Rudenko, G.N. (2002) *MuDR*/*Mu* transposons of maize. In Mobile DNA II, N.L. Craig, R. Craigie, M. Gellert, and M.A. Lambowitz, eds (Washington, DC: American Society of Microbiology), pp. 533–564.

Waterworth, W.M., Jiang, Q., West, C.E., Nikaido, M., and Bray, C.M. (2002). Characterization of Arabidopsis photolyase enzymes and analysis of their role in protection from ultraviolet-B radiation. J. Exp. Bot. **53:** 1005–1015.